2022 IEEE 5th International Electrical and Energy Conference (CIEEC) | 978-1-6654-1104-2/22/$31.00 ©2022 IEEE | DOI: 10.1109/CIEEC54735.2022.9846499

Mitigation Strategy of Sub/Supersynchronous Oscillation of PMSG Based on Additional Active Disturbance Rejection Controller

Siwen Jiang, Chongru Liu, Jianze Li
State Key Laboratory of Alternate Electrical Power System with Renewable Energy Sources
North China Electric Power University
Beijing, China
1141720594@qq.com

***Abstract*—Permanent magnet synchronous generator (PMSG) is completely decoupled from the power grid with back-to-back converters, and have been widely used in new power systems under the carbon peak and neutrality target. However, the new type of sub/super-synchronous oscillation caused by the interaction between the PMSG and the weak AC grid seriously affects the safety and stability of the power grid. Aiming at the problem of sub/super-synchronous oscillation, the frequency coupling characteristics of the sub/super-synchronous oscillation of the PMSG considering the dynamics of the phase lock loop (PLL) are analyzed firstly. Then, a PMSG sub/super-synchronous oscillation suppression strategy based on the additional active disturbance rejection controller (ADRC) is proposed. Owing to the good adaptability of ADRC to different frequency components, the sub/super- synchronous oscillation current removing the basic frequency component is suppressed to zero. Finally, a simplified equivalent model of Xinjiang power grid with wind farms was built in PSCAD/EMTDC. The simulation results show that the proposed strategy can quickly and effectively suppress the sub/super-synchronous oscillations of PMSG and maintain the stability of the wind power integrated system.**

Keywords—PMSG, sub/super-synchronous oscillations, frequency coupling, ADRC

I. Introduction

China has proposed the goal of carbon peak and carbon neutrality[1-2], and sustainable energy such as wind power and solar energy will be widely used in future power systems due to their advantages of renewable and non-polluting[3]. With the development of converter technology, PMSG that is completely decoupled from the power grid have gradually become the main development direction of wind power integrated systems[4-5]. However, the new type of sub/super-synchronous oscillation caused by the interaction between the large-scale wind farm and the grid brings new challenges to the power system[6-8]. For example, in 2015, sub/super-synchronous oscillation of multiple frequencies occurred in Xinjiang, China without series compensation[9], leading to a number of PMSGs disconnecting from the grid and HVDC blocking, which caused serious damage to the normal operation of the power grid in Northwest China. Therefore, it's great significance of studying the frequency characteristic of PMSG sub/super-synchronous oscillations and suppression schemes to improve the safety and stability of large-scale sustainable energy resources integrated system.

Targeting at the problem of sub/super-synchronous oscillation caused by wind turbine, researchers have studied and formed three kinds of solutions: 1) install physical suppression device[10-15], 2) optimize the control parameters of wind turbine converter[16,17], 3) design control strategies for suppressing sub/super-synchronous oscillation[18-29, 31-33].

The installation of physical suppression device is mainly to install flexible AC transmission system (FACTS) devices, including series suppressors and parallel suppressors. References [10-11] use static synchronous compensator (STATCOM) and unified power flow controller (UPFC) to suppress sub-synchronous resonance (SSR) of coal-fired power units. References [12-14] use thyristor-controlled series compensator (TCSC) to solve the problem of sub-synchronous oscillation caused by double feed induction generator (DFIG). Reference [15] uses STATCOM to suppress sub-synchronous oscillation of wind farms and analyzes the influence of installation position on the suppression effect. The method of adding physical suppression device realizes the suppression of sub-synchronous oscillation by directly changing the impedance characteristics of power grid, but this method adds additional physical devices, which increases a lot of investment and reduces the economy of the system.

The method of optimizing the controller parameters of wind turbine converters is to readjust the existing controller parameters, and avoid sub-synchronous oscillation. Reference [16] solves sub-synchronous oscillation caused by the interaction between grid impedance and wind turbine by optimizing the parameters of phase lock loop (PLL). Reference [17] coordinately optimizes the controller parameters of wind farm with high voltage DC transmission (HVDC) system to deal with the sub-synchronous oscillation. The method of optimizing the controller parameters of wind turbine converter does not need to add investment or change the control structure, but may reduce the stable region of the control system.

There are two modes to suppress sub/super-synchronous oscillation by using control strategy. One is to use nonlinear control method instead of wind turbine voltage and current loop control [18-23], and the other is to add a sub/super-synchronous oscillation suppression module based on the

This work was supported by the State Grid Corporation of China (Project name: Stability analysis and control strategy of offshore wind power system considering multi frequency coupling and receiving end grid characteristics; Project number: SGZJ0000KXJS1900419).

978-1-6654-1104-2/22/$31.00 ©2022 IEEE

double closed-loop vector control of the wind turbine [24-29,31-33].

The first method uses nonlinear controls such as active disturbance rejection control (ADRC) [18], quasi proportional resonance controller [19], feedback linearization control [20-22], robust/adaptive control [23] to replace the current inner loop PI control of the wind turbine, thus adapts to harmonics and voltage distortion. This method suppresses the sub/super-synchronous oscillation by reconstructing the basic control structure of wind turbine converter and using the good adaptability of nonlinear algorithm to different frequency components. However, this method needs to completely modify the control system of wind turbine, besides some nonlinear algorithms are too complex, which is not conducive to engineering practice.

Researchers have also made rich achievements in the research of additional damping control. References [24-25] design additional proportional resonance control to the grid side converter of PMSG to suppress the sub/super-synchronous frequency component. In [26-27], a hybrid sub-synchronous damping controller is added to the active and reactive outer loop control of the rotor side converter of DFIG to realize SSO suppression. Reference [28] introduces a virtual negative resistance of the sub-synchronous frequency band to the rotor side converter to enhance the damping of the wind turbine grid connected system. Reference [29] adds PID damping controller to the active loop and reactive loop of DFIG for phase compensation to optimize the amplitude frequency characteristics of system impedance and electrical damping. However, the additional damping module of these suppression strategies have many links and the parameters optimization take a long time, resulting in high delay of input and output signals. In addition, if the operating state of the system changes, the additional damping control parameters need to be retuned, which has poor adaptivity.

The ADRC [30] is decoupled from the mathematical model of the actual physical system and takes the uncertain factors in the system as disturbances for unified estimation and compensation. The control structure is simple and easy to engineering. It is very suitable for nonlinear, time-varying, coupled and uncertain sustainable energy resources integrated system. Its parameters can automatically detect and compensate the internal and external disturbances of the control object, with strong adaptability, robustness and operability. References [31-33] use additional ADRC to suppress the sub-synchronous oscillation of DFIG integrated system and photovoltaic integrated system respectively. However, there are few reports on the application of ADRC to the sub-synchronous oscillation of PMSG integrated system, except for the overall replacement of the controller in [18].

Therefore, combined with the excellent performance of ADRC, a sub/super-synchronous oscillation suppression strategy of PMSG based on additional ADRC is proposed. The main work includes the following aspects:

(1) Analysis of frequency coupling characteristics of sub/super-synchronous oscillation of PMSG

By studying the effects of the primary system and control system of the grid side converter of PMSG on the system state variables, the sub/super-synchronous oscillation coupling mechanism and frequency coupling characteristics are obtained.

(2) Sub/super-synchronous oscillation suppression strategy based on additional ADRC

An additional ADRC strategy is proposed to suppress the sub/super-synchronous oscillation of PMSG. The ADRC is used to suppress the d-axis current at PCC point of grid side converter with removed DC component to 0, thus realize the unified suppression of multi frequency sub/super-synchronous oscillation of PMSG.

II. Analysis of Sub/Super-Synchronous Oscillation Characteristics of PMSG

This section first introduces the topology and basic control strategy of PMSG, and then studies the sub/super-synchronous oscillation frequency coupling mechanism of PMSG considering the dynamics of PLL.

A. System model and classical control

Figure 1 shows the topology and control strategy of PMSG integrated system.

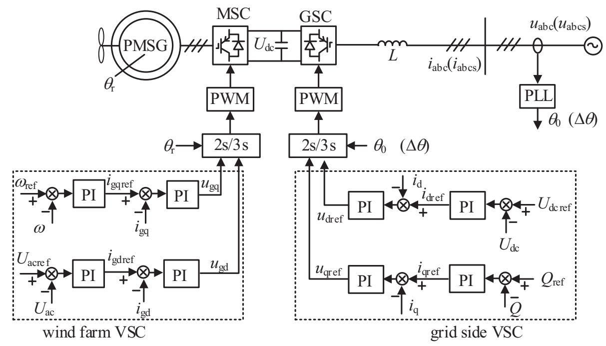

Fig. 1. Topology and control strategy of PMSG integrated system.

Where, MSC and GSC represent generator side converter and grid side converter, respectively. PCC represents a common connection point. PWM represents carrier phase shifted pulse width modulation. U_{dc} and U_{dcref} represent DC voltage and DC voltage reference value, respectively. Q and Q_{ref} represent the real time reactive power and reactive power reference value, respectively. u_{abc} and u_{abcs} represent the steady-state AC voltage at PCC and sub/super-synchronous frequency component of the AC voltage, respectively. i_{abc} and i_{abcs} represent the steady-state AC current at PCC and the sub/super-synchronous frequency component of the AC current, respectively. θ_0 represents the phase angle of steady-state AC voltage, and $\Delta\theta$ represents the disturbance of AC voltage sub/super-synchronous frequency component to the output phase angle of PLL.

PMSG composes of wind turbine, generator and back-to-back grid-connected converters. The wind turbine controls the mechanical power input of the generator, and the stator side of the generator is connected to the grid through a back-to-back converters. The back-to-back converters adopt double closed-loop vector controllers based on synchronous rotating coordinate system. PLL tracks the phase angle of AC voltage at PCC, which provides the basis for Parker transform. The d-axis outer loop of MSC adopts fixed rotor speed control, thus the PMSG can operate in maximum power point tracking (MPPT) mode by tracking the optimal speed generated by MPPT. The outer loop of q-axis of MSC adopts fixed AC voltage control to provide stable AC voltage support for the generator. The d-axis outer loop of GSC adopts fixed DC voltage control to maintain the voltage stability of back-to-back DC system. The outer loop of q-axis of GSC adopts fixed reactive power control, and the reactive reference value is usually set to 0. Based on the control scheme in Fig. 1, this paper studies the frequency coupling characteristics and suppression strategy of sub/super-synchronous oscillation of PMSG.

B. Analysis of sub/super-synchronous oscillation characteristics

The harmonic linearization method is used to study the PLL and dq-axis control system of GSC. The sub/super-synchronous frequency disturbance voltage signal u_{abcs} is added to the PCC voltage u_{abc}, thus the three-phase voltage u'_{abc} is

$$\begin{bmatrix} u'_{\mathrm{a}} \\ u'_{\mathrm{b}} \\ u'_{\mathrm{c}} \end{bmatrix} = \begin{bmatrix} U_{\mathrm{f}}\cos(\omega_0 t+\varphi_{\mathrm{f}})+U_{\mathrm{s}}\cos(\omega_{\mathrm{s}} t+\varphi_{\mathrm{s}}) \\ U_{\mathrm{f}}\cos(\omega_0 t+\varphi_{\mathrm{f}}-\frac{2\pi}{3})+U_{\mathrm{s}}\cos(\omega_{\mathrm{s}} t+\varphi_{\mathrm{s}}-\frac{2\pi}{3}) \\ U_{\mathrm{f}}\cos(\omega_0 t+\varphi_{\mathrm{f}}+\frac{2\pi}{3})+U_{\mathrm{s}}\cos(\omega_{\mathrm{s}} t+\varphi_{\mathrm{s}}+\frac{2\pi}{3}) \end{bmatrix} \tag{1}$$

where, U_{f} and φ_{f} are the amplitude and initial phase of u_{abc}, respectively. U_{s} and φ_{s} are the amplitude and initial phase of u_{abcs}, respectively. ω_{s} is the angular frequency of the sub/super-synchronous frequency component.

Once the PCC voltage superposes sub/super-synchronous frequency component, the phase angle of PLL output will no longer be the steady-state phase angle θ_0. The influence of sub/super-synchronous frequency component on phase angle can be expressed by phase angle disturbance $\Delta\theta$, i.e. $\theta=\theta_0+\Delta\theta$. Therefore, the coordinate transformation module of the three phase voltage $T_{\mathrm{dq/abc}}(\theta)$ is

$$T_{\mathrm{dq/abc}}(\theta)=\frac{2}{3}\begin{bmatrix} \cos(\theta_0+\Delta\theta) & \cos((\theta_0+\Delta\theta)-\frac{2\pi}{3}) & \cos((\theta_0+\Delta\theta)+\frac{2\pi}{3}) \\ -\sin(\theta_0+\Delta\theta) & -\sin((\theta_0+\Delta\theta)-\frac{2\pi}{3}) & -\sin((\theta_0+\Delta\theta)+\frac{2\pi}{3}) \\ \frac{1}{2} & \frac{1}{2} & \frac{1}{2} \end{bmatrix} \tag{2}$$

It can be simplified as

$$T_{\mathrm{dq/abc}}(\theta)=T_{\mathrm{dq/abc}}(\Delta\theta)\cdot T_{\mathrm{dq/abc}}(\theta_0) \tag{3}$$

where

$$T_{\mathrm{dq/abc}}(\Delta\theta)=\begin{bmatrix} \cos(\Delta\theta) & \sin(\Delta\theta) & 0 \\ -\sin(\Delta\theta) & \cos(\Delta\theta) & 0 \\ 0 & 0 & 1 \end{bmatrix} \tag{4}$$

The dq-axis component of three phase voltage u'_{abc} obtained by Park transformation varies with the output phase angle of PLL, which can be expressed as

$$\begin{bmatrix} u''_{\mathrm{d}} \\ u''_{\mathrm{q}} \end{bmatrix} = T_{\mathrm{dq/abc}}(\theta)\begin{bmatrix} u'_{\mathrm{a}} \\ u'_{\mathrm{b}} \\ u'_{\mathrm{c}} \end{bmatrix} = \begin{bmatrix} u_{\mathrm{d0}}+u_{\mathrm{ds}}+u'_{\mathrm{ds}}+u''_{\mathrm{ds}} \\ u_{\mathrm{q0}}+u_{\mathrm{qs}}+u'_{\mathrm{qs}}+u''_{\mathrm{qs}} \end{bmatrix} \tag{5}$$

where

$$\begin{cases} u'_{\mathrm{ds}}=\Delta\theta\cdot u_{\mathrm{q0}}=0 \\ u''_{\mathrm{ds}}=\Delta\theta\cdot u_{\mathrm{d0}}=\frac{1}{2}A_{\mathrm{U}}U_{\mathrm{s}}\cos(-\varphi_{A_{\mathrm{U}}}-\varphi_{\mathrm{s}}+\varphi_{\mathrm{f}}+\frac{\pi}{2})+ \\ \quad \frac{1}{2}A_{\mathrm{U}}U_{\mathrm{s}}\cos(2(\omega_0-\omega_{\mathrm{s}})t+\varphi_{A_{\mathrm{U}}}-\varphi_{\mathrm{s}}+\varphi_{\mathrm{f}}+\frac{\pi}{2}) \\ u'_{\mathrm{qs}}=-\Delta\theta\cdot u_{\mathrm{d0}}=-A_{\mathrm{U}}U_{\mathrm{f}}\cos((\omega_0-\omega_{\mathrm{s}})t)+\varphi_{A_{\mathrm{U}}}) \\ u''_{\mathrm{qs}}=-\Delta\theta\cdot u_{\mathrm{q0}}=-\frac{1}{2}A_{\mathrm{U}}U_{\mathrm{s}}\cos(-\varphi_{A_{\mathrm{U}}}-\varphi_{\mathrm{s}}+\varphi_{\mathrm{f}})+ \\ \quad \frac{1}{2}A_{\mathrm{U}}U_{\mathrm{s}}\cos(2(\omega_0-\omega_{\mathrm{s}})t+\varphi_{A_{\mathrm{U}}}-\varphi_{\mathrm{s}}+\varphi_{\mathrm{f}}) \end{cases} \tag{6}$$

It can be seen from (5) and (6) that after the sub/super-synchronous frequency component u_{abcs} is introduced into the PCC voltage, the dq-axis components generated by Park transformation contain not only the DC component, but also the AC component with frequency of (ω_0 - ω_{s}). Similarly, the dq-axis components of the current after Park transformation can be expressed as

$$\begin{bmatrix} i''_{\mathrm{d}} \\ i''_{\mathrm{q}} \end{bmatrix} = T_{\mathrm{dq/abc}}(\theta)\begin{bmatrix} i_{\mathrm{a}}+i_{\mathrm{as}} \\ i_{\mathrm{b}}+i_{\mathrm{bs}} \\ i_{\mathrm{c}}+i_{\mathrm{cs}} \end{bmatrix} = \begin{bmatrix} i_{\mathrm{d0}}+i_{\mathrm{ds}}+i'_{\mathrm{ds}}+i''_{\mathrm{ds}} \\ i_{\mathrm{q0}}+i_{\mathrm{qs}}+i'_{\mathrm{qs}}+i''_{\mathrm{qs}} \end{bmatrix} \tag{7}$$

where

$$\begin{cases} i'_{\mathrm{ds}}=\Delta\theta\cdot i_{\mathrm{q0}}=0 \\ i''_{\mathrm{ds}}=\Delta\theta\cdot i_{\mathrm{d0}}=\frac{1}{2}A_{\mathrm{I}}I_{\mathrm{s}}\cos(-\varphi_{A_{\mathrm{I}}}-\varphi_{\mathrm{Is}}+\varphi_{\mathrm{If}}+\frac{\pi}{2})+ \\ \quad \frac{1}{2}A_{\mathrm{I}}I_{\mathrm{s}}\cos(2(\omega_0-\omega_{\mathrm{s}})t+\varphi_{A_{\mathrm{I}}}-\varphi_{\mathrm{Is}}+\varphi_{\mathrm{If}}+\frac{\pi}{2}) \\ i'_{\mathrm{qs}}=-\Delta\theta\cdot i_{\mathrm{d0}}=-A_{\mathrm{I}}I_{\mathrm{f}}\cos((\omega_0-\omega_{\mathrm{s}})t)+\varphi_{A_{\mathrm{I}}}) \\ i''_{\mathrm{qs}}=-\Delta\theta\cdot i_{\mathrm{q0}}=-\frac{1}{2}A_{\mathrm{I}}I_{\mathrm{s}}\cos(-\varphi_{A_{\mathrm{I}}}-\varphi_{\mathrm{Is}}+\varphi_{\mathrm{If}})+ \\ \quad \frac{1}{2}A_{\mathrm{I}}I_{\mathrm{s}}\cos(2(\omega_0-\omega_{\mathrm{s}})t+\varphi_{A_{\mathrm{I}}}-\varphi_{\mathrm{Is}}+\varphi_{\mathrm{If}}) \end{cases} \tag{8}$$

where, I_{f} and φ_{If} are the amplitude and initial phase of fundamental frequency current i_{abc}, respectively. I_{s} and φ_{Is} are the amplitude and initial phase of sub/super-synchronous frequency i_{abcs}, respectively.

According to the control block of GSC shown in Fig. 1, dq-axis voltage reference values are

$$\begin{cases} u_{dref} = (i_{dref} - i_d)(K_{pd} + \frac{K_{id}}{s}) - \omega_0 L i_q + u_d \\ u_{qref} = (i_{qref} - i_q)(K_{pq} + \frac{K_{iq}}{s}) + \omega_0 L i_d + u_q \end{cases} \quad (9)$$

The small signal equation of (9) is:

$$\begin{cases} \Delta u_{dref} = -\Delta i_d \cdot (K_{pd} + \frac{K_{id}}{s}) - \omega_0 L \Delta i_q + \Delta u_d \\ \Delta u_{qref} = -\Delta i_q \cdot (K_{pq} + \frac{K_{iq}}{s}) + \omega_0 L \Delta i_d + \Delta u_q \end{cases} \quad (10)$$

where, K_{pd}, K_{id}, K_{pq} and K_{iq} are the proportional and integral coefficients of dq-axis inner loop PI controller respectively.

Substituting (10) with (6) and (8), the dq-axis voltage reference value u''_{dref} and u''_{qref} considering the phase angle disturbance of PLL can be derived as

$$\begin{cases} u''_{dref} = u_{d0} + A_{d1}\cos((\omega_0 - \omega_s)t + \varphi_{Ad1}) \\ \qquad + A_{d2}\cos(2(\omega_0 - \omega_s)t + \varphi_{Ad2}) \\ u''_{qref} = u_{q0} + A_{q1}\cos((\omega_0 - \omega_s)t + \varphi_{Aq1}) \\ \qquad + A_{q2}\cos(2(\omega_0 - \omega_s)t + \varphi_{Aq2}) \end{cases} \quad (11)$$

where, A_{d2} and A_{q2} are the reference value of amplitude of dq-axis voltage with frequency of $2(\omega_0 - \omega_s)$, and φ_{Ad2} and φ_{Aq2} are the reference value of initial phase of voltage with frequency of $2(\omega_0 - \omega_s)$.

The three-phase voltage instruction value u''_{abcref} can be obtained by inverse Parker transformation of dq-axis voltage reference value

$$\begin{bmatrix} u''_{aref} \\ u''_{bref} \\ u''_{cref} \end{bmatrix} = T_{abc/dq}(\theta) \begin{bmatrix} u''_{dref} \\ u''_{qref} \end{bmatrix} \quad (12)$$

The three-phase voltage instruction value in (12) can be expanded into

$$\begin{bmatrix} u''_{aref} \\ u''_{bref} \\ u''_{cref} \end{bmatrix} = \begin{bmatrix} U_f \cos(\omega_0 t + \varphi_a) + A_{as1}\cos((\omega_0 - \omega_s \pm \omega_0)t + \varphi_{as1}) \\ + A_{as2}\cos((2(\omega_0 - \omega_s) \pm \omega_0)t + \varphi_{as2}) \\ U_f \cos(\omega_0 t + \varphi_a + \frac{2\pi}{3}) + A_{as1}\cos((\omega_0 - \omega_s \pm \omega_0)t + \varphi_{as1} + \frac{2\pi}{3}) \\ + A_{as2}\cos((2(\omega_0 - \omega_s) \pm \omega_0)t + \varphi_{as2} + \frac{2\pi}{3}) \\ U_f \cos(\omega_0 t + \varphi_a - \frac{2\pi}{3}) + A_{as1}\cos((\omega_0 - \omega_s \pm \omega_0)t + \varphi_{as1} - \frac{2\pi}{3}) \\ + A_{as2}\cos((2(\omega_0 - \omega_s) \pm \omega_0)t + \varphi_{as2} - \frac{2\pi}{3}) \end{bmatrix} \quad (13)$$

Considering the disturbance of the output phase angle of the PLL, the new sub/super-synchronous frequency voltage component and its dual frequency component is generated due to the action of PMSG control links.

III. Suppression of Sub/Super-Synchronous Oscillation Based on ADRC

Aiming at the problem of sub/super-synchronous frequency coupling of PMSG, based on the study of the mathematical model of ADRC, an additional ADRC strategy for GSC is proposed to suppress multiple coupled frequency components in sub/super-synchronous oscillation.

A. *Mathematical model of ADRC*

ADRC is a new control technology evolved from classical PID control technology. Compared with the linear combination of proportion, integral and differential commonly used in classical PID control, ADRC abandons the integral link and adopts nonlinear feedback structure to replace the linear combination of proportion, integral and differential, which fundamentally improves the inherent defects of PID.

For a second-order control system with external disturbances, its mathematical model can be described as

$$\begin{cases} x_1' = x_2 \\ x_2' = f_0(x_1, x_2) + \omega(t) + bu \\ y = x_1 \end{cases} \quad (14)$$

where, x_1 and x_2 are the state variables of the control system. $\omega(t)$ is the sum of the unknown part of the model and the disturbance. f_0 is a known part of the model, and it can also be included in $\omega(t)$, that is, the system is considered unknown. b is the amplification factor of the control quantity.

For the second-order system state equation in (14), a second-order ADRC controller can be designed to control the system. The ADRC structural diagram is shown in Fig. 2, which mainly includes three parts: extended state observer (ESO), tracking differentiator (TD), nonlinear state error feedback and disturbance estimation compensation (NLSEF).

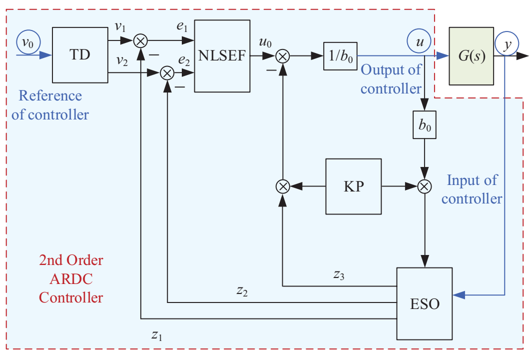

Fig. 2. Structure of ADRC.

According to the control target v_0, TD reasonably arranges the transition process v_1 and extracts its error differential signal v_2, so as to reduce the initial error and balance the demand for rapidity and overshoot in the transition process. The mathematical model of TD is

$$\begin{cases} e_0(k) = v_1(k) - v_0(k) \\ f_{\mathrm{h}} = f_{\mathrm{han}}(e_0(k), v_2(k), r_0, h_0) \\ v_1(k+1) = v_1(k) + hv_2(k) \\ v_2(k+1) = v_2(k) + hf_{\mathrm{h}} \end{cases} \tag{15}$$

where, h refers to the simulation step size, r_0 refers to the speed factor, h_0 refers to the filter factor. $f_{\mathrm{han}}(p_1,p_2,r,h)$ is the synthesis function of discrete fastest control, which is defined as

$$\begin{cases} d = rh, \quad d_0 = hd, \quad q = p_1 + hp_2 \\ a_0 = \sqrt{d^2 + 8r|q|}, \quad \mathrm{sign}(x) = \begin{cases} x/|x| & x \neq 0 \\ 0 & x = 0 \end{cases} \\ a = \begin{cases} p_2 + \dfrac{(a_0 - d)}{2}\mathrm{sign}(q) & |q| > d_0 \\ p_2 + \dfrac{q}{h} & |q| \leq d_0 \end{cases} \\ f_{\mathrm{han}} = -\begin{cases} r\mathrm{sign}(a) & |a| > d \\ r\dfrac{a}{d} & |a| \leq d \end{cases} \end{cases} \tag{16}$$

where, d and d_0 control the linear segment length of f_{han}, q, a and a_0 are internal variables, and sign(x) is a symbolic function.

ESO tracks the state variables x_1 and x_2 through the system output variable y and the control variable u, which are expressed as z_1 and z_2, and expands the disturbance $\omega(t)$ affecting the control output into a new state variable z_3. The nonlinear ESO considering the known part of the system is

$$\begin{cases} e(k) = z_1(k) - y(k) \\ f_{\mathrm{e}} = f_{\mathrm{al}}(e(k), \alpha_1, \delta) \\ f_{\mathrm{e1}} = f_{\mathrm{al}}(e(k), \alpha_2, \delta) \\ z_1(k+1) = z_1(k) + h(z_2(k) - \beta_{01}e(k)) \\ z_2(k+1) = z_2(k) + h(f_0(z_1(k), z_2(k)) \\ \qquad + z_3(k) - \beta_{02}f_{\mathrm{e}} + b_0u(k)) \\ z_3(k+1) = z_3(k) + h(-\beta_{03}f_{\mathrm{e1}}) \end{cases} \tag{17}$$

where, β_{01}, β_{02}, β_{03} is the gain factor. $f_{\mathrm{al}}(e,\alpha,\delta)$ is a continuous power function with linear segments near the origin, which can avoid high frequency flutter phenomenon.

$$f_{\mathrm{al}}(e, \alpha, \delta) = \begin{cases} \dfrac{e}{\delta^{1-\alpha}} & |e| \leq \delta \\ |e|^{\alpha}\,\mathrm{sign}(e) & |e| > \delta \end{cases} \tag{18}$$

where, δ is the linear interval length, α is a power parameter, usually $0<\alpha\leq 1$.

NLSEF combines the state error information of TD and ESO, and configures appropriate feedback control to suppress system disturbance and improve system operation characteristics. NLSEF can be expressed as

$$\begin{cases} e_1(k) = v_1(k) - z_1(k), e_2(k) = v_2(k) - z_2(k) \\ u_0(k) = k(e_1(k), e_2(k), p) \end{cases} \tag{19}$$

where, $k(e_1(k),e_2(k))$ refers to a variety of feedback functions (linear or nonlinear functions can be used), and p is the feedback form parameter set.

The feedback law of the controller adopts the fastest feedback function $u_0 = -f_{\mathrm{han}}(e_1, ce_2, r, h_1)$ with damping factor. c is the damping factor, r is the control gain, and h_1 is the speed factor.

The error feedback value u_0 in (19) is superimposed with the disturbance estimator z_3 of ESO to obtain the final control value.

$$u(k) = \frac{u_0(k) - f_0(z_1(k), z_2(k)) - z_3(k)}{b_0} \tag{20}$$

where, b_0 is the compensation factor.

B. Suppression strategy of sub/super-synchronous oscillation of PMSG

Based on the principle of second-order ADRC, an additional ADRC strategy for PMSG is proposed to suppress the sub/super-synchronous oscillation. The structure of the proposed suppression strategy is shown in Fig. 3.

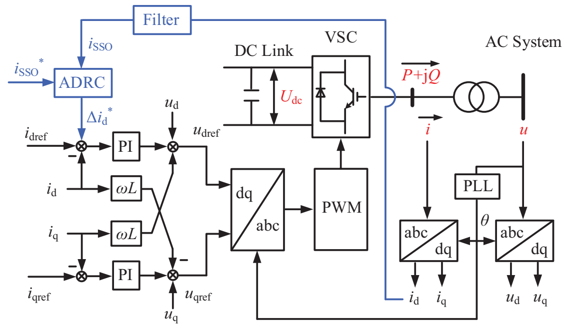

Fig. 3. Structure of suppression strategy of sub/super-synchronous oscillation of PMSG.

The sub/super-synchronous oscillation suppression strategy collects the d-axis current component of PCC of GSC after Park transformation, and uses the first-order filter shown in (21) to remove the DC component in the d-axis current, so as to obtain the oscillation current i_{sso} including all sub/super-synchronous frequency components. Then set the sub/super-synchronous current reference value i_{sso}^* to 0, input i_{sso} as the controlled variable into the second-order ADRC controller, and the output of the ADRC controller is superimposed on the d-axis current reference value of GSC to form a control closed loop. Using the good adaptability of ADRC controller to different frequency band components, the sub/super-synchronous current i_{sso} is suppressed to 0 to eliminate the sub/super-synchronous oscillation.

$$G(s)=\frac{1}{1+Ts} \tag{21}$$

where T is the first-order inertial time constant, usually 0.0005s.

When the wind turbine works normally, the system state variable does not contain the sub/super-synchronous frequency component, and the ADRC is locked. The PMSG control system operates normally according to the reference value given by the dispatching center. After the sub/super-synchronous oscillation occurs in the system, the additional ADRC starts up when the sub/super-synchronous oscillation current i_{sso} amplitude exceeds 0.05 p.u.. Under the joint action of double closed-loop vector control and additional ADRC, the PMSG suppresses the sub/super-synchronous current to 0, so as to maintain the normal operation of the PMSG.

C. Control parameter tunning method

Since there are clear boundaries in each link of ADRC, the parameters of each link can be tunned separately by modular scheme according to the separation principle to simplify the parameter design process.

The filter factor h_0 in TD can be used to suppress noise in the input differential signal. After the simulation step h is determined, increasing h_0 can effectively improve the filtering effect. For a fixed reference input, filtering is not required, and h_0 can be made equal to h. The larger r_0 is, the closer TD output is to the reference signal, but a too large r_0 will lead to differential signal oscillation. The smaller r_0, the smoother TD output tracking reference signal. r_0 can be set as 1000 in this paper.

The main parameters in ESO include α_1, α_2, δ, β_{01}, β_{02}, β_{03}. If δ is too large, the linear working area is too large, which affects the performance of the controller. While if δ is too small, it is easy to occur high-frequency flutter. Therefore,α_1, α_2, δ determines the nonlinearity of ESO and has a great influence on the tunning of other parameters. So α_1, α_2, δ gives priority to tuning, usually taking α_1 equals 0.5, α_2 equals 0.25 and δ equals h. The gain coefficient β_{01}, β_{02}, β_{03} affect the observation effect of ESO, and must meet the stability requirements of ESO. After h, α_1, α_2, δ is determined, ESO parameters can be designed by bandwidth tunning method [31].

$$\begin{cases}\beta_{01}=3m_0\\ \alpha_1\beta_{02}=3m_0^2\\ \alpha_2\beta_{03}=m_0^3\end{cases} \tag{22}$$

where m_0 refers to observer bandwidth. In order to effectively observe the total disturbance of the system at sub/super-synchronous frequency, m_0 should be increased as much as possible on the premise of observer stability. This paper takes β_{01}=1/h, and substitute it into (22).

$$\begin{cases}\beta_{01}=\dfrac{1}{h}\\ \beta_{02}=\dfrac{1}{3\alpha_1 h^2}\\ \beta_{03}=\dfrac{1}{27\alpha_2 h^3}\end{cases} \tag{23}$$

The compensation factor b_0 in disturbance estimation compensation is theoretically the amplification factor b. However, b is usually unknown, so it is necessary to estimate b_0 near the true value of b. Since ADRC algorithm requires very low estimation accuracy of b_0, the influence of relative error less than 30% on control effect can be ignored. The trial-and-error method [30] can be used to select b_0.

The suppression strategy of sub/super-synchronous oscillation of PMSG based on the additional ADRC is put into use only after the occurrence of sub/super-synchronous oscillation, which does not affect the normal control and operation of wind turbine integrated system. In the process of oscillation suppression, the characteristics of strong adaptability and good robustness of ADRC are fully utilized. Meanwhile, the parameter tuning method of ADRC proposed in this paper has clear structure and good engineering practice value.

IV. Simulation

Based on the simulation model of Xinjiang grid with PMSG wind farm in PSCAD/EMTDC, this section verifies the effectiveness of the sub/super-synchronous oscillation suppression strategy of PMSG based on additional ADRC.

A. Simulation model

Figure 4 shows the simplified equivalent model of Xinjiang grid with PMSG wind farm, in which node A is connected to two wind farms, and nodes B and C are connected to one wind farm respectively. Those wind farms connect to the 750kV main grid through node D. In order to simplify analysis, assuming that the rated capacity of each wind turbine is the same, which is 5.2MW, and the equivalent method of capacity weighting is used to model the wind farms. The number of wind turbines included in wind farms a_1, a_2, b and c is 61, 16, 84 and 118 respectively.

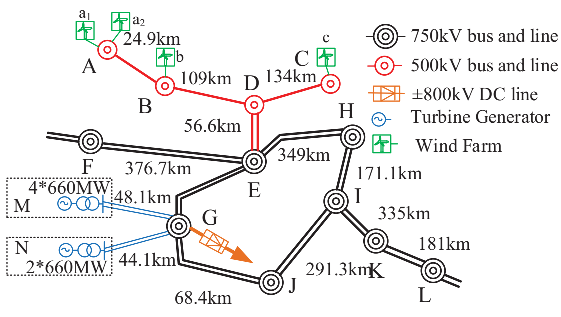

Fig. 4. Simplified equivalent model of Xinjiang grid with PMSG.

The system parameters and control parameters of a wind turbine are shown in Table I.

TABLE I. PARAMETERS OF PMSG WIND FARM

Symbol	Quantity /unit	Symbol	Quantity /unit	Symbol	Quantity /unit
U_{AC}	0.69/kV	k_{pdc}	10/p.u.	k_{pd}	5/p.u.
U_{dc}	1.45/kV	k_{idc}	0.05/p.u.	k_{id}	0.01/p.u.
V_W	12/m/s	k_{pQ}	0.1/p.u.	k_{pq}	1.2/p.u.
f	50/Hz	k_{iQ}	0.1/p.u.	k_{iq}	0.025/p.u.

where, V_W refers to the rated wind speed, f refers to the rated frequency, k_{pQ} and k_{iQ} refer to the proportional and integral parameters of the reactive outer loop PI controller of GSC.

B. Verification of oscillation suppression strategy

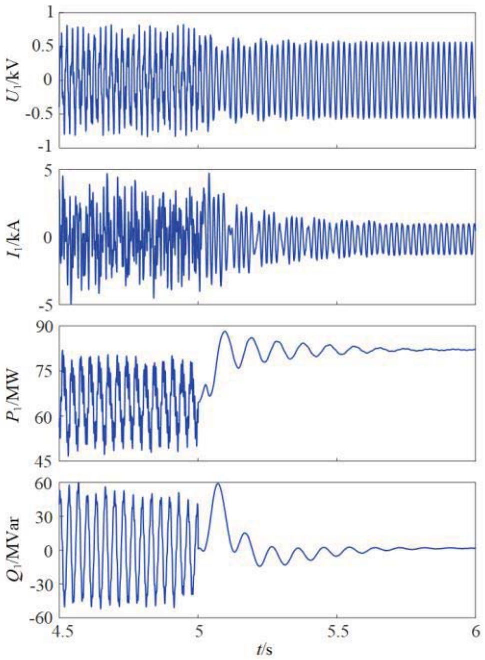

Fig. 5. System states of PCC of wind farm.

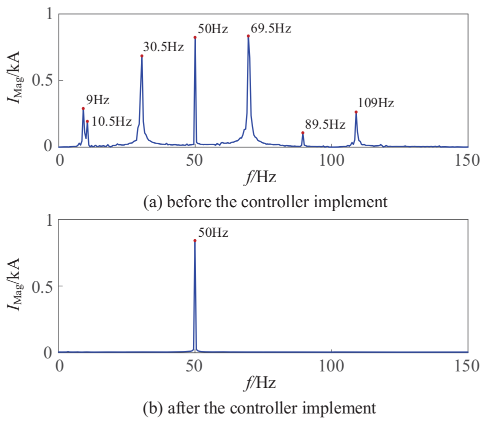

Fig. 6. Frequency spectrum analysis of PCC current.

The rated wind speed of the PMSG wind farm a_2 connected to node A is 12m/s. when the wind speed becomes 7m/s, the wind turbine integrated system occurs sub/super-synchronous oscillation. When t = 5s, the proposed sub/super-synchronous oscillation suppression strategy is put into operation. The simulation results of AC voltage, AC current, active power, and reactive power at PCC of the wind farm are showed in Fig. 5. Figure 6 shows the frequency spectrum analysis results of AC circuit before and after the suppression strategy puts into operation.

It can be seen from Fig. 5 that when the PMSG undergoes sub/super-synchronous oscillation, there is obvious oscillation in the AC voltage, AC current, active power and reactive power at PCC. The frequency spectrum of A phase AC current is analyzed. As shown in Fig. 6 (a), there are three groups of sub/super-synchronous dual oscillation frequency components such as 9/109Hz, 10.5/89.5Hz and 30.5/69.5Hz in the system. Since only the positive half plane spectrum is used in Fourier decomposition, 9Hz in 9/109Hz is the negative sequence frequency, that is, the oscillation frequency of this group is actually -9/109Hz. The three groups of sub/super-synchronous oscillation frequencies of -9/109Hz, 10.5/89.5Hz and 30.5/69.5Hz are symmetrical about the fundamental frequency of 50Hz, which proves the conclusion that PMSG produces a new oscillation frequency and its dual frequency under the disturbance of sub/super-synchronous oscillation is correct in section II.B.

When the sub/super-synchronous oscillation suppression strategy is put into operation, the sub/super-synchronous current is quickly suppressed to 0 under the action of ADRC, and the active power, reactive power and AC voltage also quickly return to normal state. The spectrum analysis results in Fig. 6(b) show that only the fundamental frequency component remains in the PCC current.

V. CONCLUSION

Aiming at the problem of sub/super-synchronous frequency coupling when sub-synchronous oscillation occurs in PMSG, a suppression strategy of sub/super-synchronous oscillation of PMSG based on additional ADRC is proposed in this paper. The conclusions are as follows:

(1) The frequency coupling and characteristics of sub/super-synchronous oscillation of PMSG are analyzed theoretically. When the PMSG has sub/super-synchronous oscillation, the output phase angle of the PLL is disturbed, resulting in a new oscillation frequency and its dual frequency.

(2) The sub/super-synchronous oscillation suppression strategy based on additional ADRC can suppress the current of multiple groups sub/super-synchronous oscillation frequencies at the same time by using the adaptability of ADRC to multiple frequency components. Meanwhile, this method has no effect on the normal operation of the PMSG control system, and is only put into use after the oscillation occurs.

(3) The simplified equivalent model of Xinjiang grid with PMSG is built in PSCAD/EMTDC, and the effectiveness of sub/super-synchronous oscillation suppression strategy is verified. The simulation results show that the proposed control strategy can suppress sub/super-synchronous oscillation quickly and effectively.

References

[1] Q. Li, W. Yu, J. Zhao, "Key technologies for the safe operation of wind and solar power generation equipment in support of the peak CO_2 emissions and carbon neutrality policy," High Voltage Engineering, vol. 47, no. 9, pp. 3047–3060, September 2021.

[2] J. Ding, X. Fang, Y. Song, et al, "Conception of electricity and hydrogen integrated energy network for renewable energy transmission in western china under background of carbon neutralization," Automation of Electric Power Systems, vol. 45, no. 24, pp. 1–9, December 2021.

[3] J. Wang, A. AlShelahi, M. You, et al, "Integrative density forecast and uncertainty quantification of wind power generation," IEEE Transactions on Sustainable Energy, vol. 12, no. 4, pp. 1864-1875, October 2021.

[4] Z. Zheng, Q. Xie, C. Huang, et al, "Superconducting technology based fault ride through strategy for PMSG-based wind turbine generator: a comprehensive review," IEEE Transactions on Applied Superconductivity, vol. 31, no. 8, pp. 1-6, November 2021.

[5] M. K. K. Prince, M. T. Arif, A. Gargoom, et al, "Modeling, parameter measurement, and control of PMSG-based grid-connected wind energy conversion system," Journal of Modern Power Systems and Clean Energy, vol. 9, no. 5, pp. 1054-1065, September 2021.

[6] B. Liu, Z. Li, X. Dong, et al, "Impedance modeling and controllers shaping effect analysis of PMSG wind turbines," IEEE Journal of Emerging and Selected Topics in Power Electronics, vol. 9, no. 2, pp. 1465-1478, April 2021.

[7] W. Du, Y. Wang, X. Wang, et al, "Magnifying effect of weak grid connection for a PMSG to induce torsional sub-synchronous oscillations under the condition of open-loop modal resonance," IET Renewable Power Generation, vol. 14, no. 4, pp. 580–590, February 2020.

[8] S. Zhao, N. Wang, R. Li, et al, "Sub-synchronous control interaction between direct-drive PMSG-based wind farms and compensated grids," International Journal of Electrical Power & Energy Systems, vol. 109, pp. 609–617, July 2019.

[9] H. Liu, X. Xie, J. He, et al, "Subsynchronous interaction between direct-drive PMSG based wind farms and weak ac networks," IEEE Transactions on Power Systems, vol. 32, no. 6, pp. 4708-4720, November 2017.

[10] G. Wang, H. Sun, X. Zhu, et al, "Theory and simulation of STATCOM supplementary voltage control to damp subsynchronous resonance," Automation of Electric Power Systems, vol. 37, no. 11, pp. 33–38, June 2013.

[11] X. Zhu, M. Jin, J. Li, et al, "Theory and simulation of supplementary damping control for unified power flow controller to mitigate subsynchronous resonance," Automation of Electric Power Systems, vol. 40, no. 16, pp. 44–48+97, August 2016.

[12] H. A. Mohammadpour, E. Santi, "Modeling and control of gate-controlled series capacitor interfaced with a DFIG-based wind farm," IEEE Transactions on Industrial Electronics, vol. 62, no. 2, pp. 1022-1033, February 2015.

[13] R. K. Varma, S. Auddy, Y. Semsedini, "Mitigation of subsynchronous resonance in a series-compensated wind farm using FACTS controllers," IEEE Transactions on Power Delivery, vol. 23, no. 3, pp. 1645-1654, July 2008.

[14] L. Piyasinghe, Z. Miao, J. Khazaei, et al, "Impedance model-based SSR analysis for TCSC compensated type-3 wind energy delivery systems," IEEE Transactions on Sustainable Energy, vol. 6, no. 1, pp. 179-187, January 2015.

[15] Y. Wang, L. Wang, Q. Jiang, "STATCOM based supplementary damping mitigation strategy for subsynchronous control interaction in wind farms," Automation of Electric Power Systems, vol. 43, no. 15, pp. 49–55, August 2019.

[16] C. Zhang, S. Wang, G. He, et al, "Analysis of sub-synchronous oscillation of full-converter wind farm based on sequence impendance and an optimized design method for PLL parameters," Proceedings of the CSEE, vol. 37, no. 23, pp. 6757–6767, December 2017.

[17] Y. Sheng, T. Lin, B. Chen, et al, "Coordination and optimization of controller parameters for subsynchronous/super-synchronous oscillation in new energy delivery systems," Transactions of China Electrotechnical society, vol. 34, no. 5, pp. 983–993, March 2019.

[18] B. Gao, Y. Yi, B. Shao, et al, "Subsynchronous oscillation mitigation strategy based on ADRC for D-PMSGs based wind farm," Electric Power Automation Equipment, vol. 40, no. 9, pp. 148–155, September 2020.

[19] H. Xu, Y. Teng, X. Wang, "A control strategy combining repetitive control and Quasi-PR control for PMSG grid-side converter," Power Systems Protection and Control, vol. 46, no. 8, pp. 95–102, April 2018.

[20] B. Shao, S. Zhao, B. Gao, et al, "Sub-synchronous oscillation mitigation strategy of direct-drive wind farms via VSC-HVDC system based on feedback linearization sliding mode control," Proceedings of the CESS, vol. 41, no. 9, pp. 3090–3105, May 2021.

[21] M. A. Chowdhury, G. M. Shafiullah, "SSR mitigation of series-compensated DFIG wind farms by a nonlinear damping controller using partial feedback linearization," IEEE Transactions on Power Systems, vol. 33, no. 3, pp. 2528-2538, May 2018.

[22] M. A. Chowdhury, M. A. Mahmud, W. Shen et al, "Nonlinear controller design for series-compensated DFIG-based wind farms to mitigate subsynchronous control interaction," IEEE Transactions on Energy Conversion, vol. 32, no. 2, pp. 707-719, June 2017.

[23] J. Yang, T. Wang, J. Bi, et al, "Robust damping control of subsynchronous oscillation in power system with direct-drive wind turbines," Automation of Electric Power Systems, vol. 44, no. 3, pp. 56–65, February 2020.

[24] P. Zhou, R. Song, G. Li, et al, "Subsynchronous oscillation mitigation method for wind turbines based on additional proportional resonance control," Proceedings of the CESS, vol. 41, no. 11, pp. 3797–3806, June 2021.

[25] J. Lv, P. Dong, G. Shi, et al, "Subsynchronous oscillation and its mitigation of MMC-based HVDC with large doubly-fed induction generator-based wind farm integration," Proceedings of the CESS, vol. 35, no. 19, pp. 4852–4860, October 2015.

[26] B. Gao, R. Li, D. Yang, et al, "Damping characteristics and countermeasure of DFIG sub-synchronous oscillation," Electric Power Automation Equipment, vol. 35, no. 12, pp. 11–20, December 2015.

[27] B. Wang, J. Lu, J. Gong, et al, "A method to suppress sub-synchronous oscillation of wind farm composed of doubly fed induction generators with additional rotor side control," Power System Technology, vol. 37, no. 9, pp. 2580–2584, September 2013.

[28] L. Zhu, X. Xu, Y. Hou, et al, "A suppression strategy for DFIG subsynchronous oscillation based on broadband rotor additional damping," Power System Protection and Control, vol. 46, no. 2, pp. 37–42, January 2018.

[29] H. Li, Y. Chen, B. Zhao, et al, "Analysis and control strategies for depressing system sub-synchronous oscillation of DFIG-based wind farms," Proceedings of the CSEE, vol. 35, no. 7, pp. 1613–1620, April 2015.

[30] J. Han, Active Disturbance Rejection Control Technique-the Technique for Estimating and Compensating the Uncertainties. Beijing, China: National Defense Industry Press, 2008.

[31] B, Gao, L. Yao, "Supplementary damping control of SSO based on fuzzy active disturbance rejection control for photovoltaic-thermal-bundled system transmitted by series compensation," Electric Power Automation Equipment, vol. 38, no. 7, pp. 121-127, July 2018.

[32] Y. Bi, T. Liu, L. Zhao et al, "DC additional damping control of subsynchronous oscillation based on improved active disturbance rejection control for wind-thermal-bundled power system," Electric Power Automation Equipment, vol. 38, no. 11, pp. 174-180, November 2018.

[33] Y. Ma, Y. Jiang, L. Cheng et al, "An ADRC additional damping control strategy research on low frequency oscillation suppression of photovoltaic plants," Power System Technology, vol. 41, no. 6, pp. 1741-1747, June 2017.